

An advanced approach to finding magnetometer zero levels in the interplanetary magnetic field

This article has been downloaded from IOPscience. Please scroll down to see the full text article.

2008 Meas. Sci. Technol. 19 055104

(<http://iopscience.iop.org/0957-0233/19/5/055104>)

[The Table of Contents](#) and [more related content](#) is available

Download details:

IP Address: 128.32.147.236

The article was downloaded on 12/03/2010 at 23:15

Please note that [terms and conditions apply](#).

An advanced approach to finding magnetometer zero levels in the interplanetary magnetic field

H K Leinweber¹, C T Russell¹, K Torkar², T L Zhang²
and V Angelopoulos¹

¹ Institute of Geophysics and Planetary Physics, University of California, 405 Hilgard Ave., Los Angeles, CA 90095-1567, USA

² Space Research Institute, Austrian Academy of Sciences, Schmiedlstrasse 6, 8042 Graz, Austria

E-mail: hleinweber@igpp.ucla.edu

Received 10 November 2007, in final form 12 March 2008

Published 21 April 2008

Online at stacks.iop.org/MST/19/055104

Abstract

For a magnetometer that measures weak interplanetary fields, the in-flight determination of zero levels is a crucial step of the overall calibration procedure. This task is more difficult when a time-varying magnetic field of the spacecraft interferes with the surrounding natural magnetic field or when the spacecraft spends only short periods of time in the interplanetary magnetic field. Thus it is important to examine the algorithms by which these zero levels are determined, and optimize them. We find that the method presented by Davis and Smith (1968 *EOS Trans. AGU* **49** 257) has significant mathematical advantages over that published by Belcher (1973 *J. Geophys. Res.* **71** 5509) as well as over the correlation technique published by Hedgecock (1975 *Space Sci. Instrum.* **1** 83–90). We present an alternative derivation of the Davis–Smith method which illustrates that it is also a correlation technique. It also works with first differences as well as filtered data as input. In contrast to the postulate by Hedgecock (1975 *Space Sci. Instrum.* **1** 83–90), we find that using first differences in general provides no advantage in determining the zero levels. Our new algorithm obtains zero levels by searching for pure rotations of the interplanetary magnetic field, with a set of sophisticated selection criteria. With our algorithm, we require shorter periods (of the order of a few hours, depending on solar wind conditions) of interplanetary data for accurate zero level determination than previously published algorithms.

Keywords: magnetometer calibration, interplanetary magnetic field, solar wind, Alfvén waves

1. Introduction

Post-launch spacecraft magnetometer zero levels can differ from their pre-launch values for many reasons. Some of the most common issues are temperature changes of the sensor and the electronics, varying magnetic fields of the spacecraft due to electric currents or magnetic permeability, aging of electronic parts, exposure to strong radiation and other causes. See Acuña (2002) for a general review on space-based magnetometers. A historical review on measurements of the interplanetary magnetic field can be found in Ness and Burlaga (2001). Also see Snare (1998) for a historical review on vector magnetometry in space. For a spinning spacecraft, the zero

levels of the component axes that lie in the spin plane can be estimated by averaging in the spinning spacecraft frame over many spin periods when gains and angles are known to high enough precision and the magnetic field is constant during the averaging period. However, spacecraft-generated AC magnetic fields at the spin frequency in the spinning frame will cause erroneous zero levels in the despun spacecraft frame that cannot be found by averaging. For a discussion of the calibration of magnetometers on a spinning spacecraft such as determining relative gains and orientations, see Kepko *et al* (1996). Farrell *et al* (1995) is another reference on the calibration of magnetometers on a spinning spacecraft, but it omits relative gains. A commonly used term for the zero level

is offset. We will use both terms interchangeably throughout this paper.

In the solar wind, a simple method that can be used to determine constant or extremely slowly varying zero levels is averaging of the magnetic field values over a few solar rotations. The averages of all three component axes should be zero since the divergence of B is zero, and the configuration of the solar magnetic field should not be correlated with the spacecraft location. However, we note that there are field configurations that can be symmetric about the Sun's rotation axis such as those associated with the $g_1^0, g_2^0, g_3^0, \dots$ coefficients of the Legendre polynomial expansion (see, for example, Altschuler *et al* (1977) and references therein); so this technique is not foolproof. Furthermore, this technique requires that the spacecraft stays in the interplanetary magnetic field continually and returns an average zero level at most only monthly. It is desirable to determine offsets much more often and to not rely on the Sun having a favorable magnetic configuration. Fluctuations of the interplanetary field are primarily changes in the direction rather than in the magnitude so that the field magnitude is more constant than any of its three component axes (Ness *et al* 1964). See also power spectra and histograms in Coleman (1966). Fortunately, the Alfvénic nature (Belcher *et al* 1969) of the solar wind fluctuations allows us to determine offsets comparatively rapidly, much faster than once per month.

There are three documented methods for finding zero levels in the interplanetary magnetic field, based on the above-described property of the interplanetary magnetic field to determine slowly changing zero levels. The first method developed is called the Davis–Smith method (Davis and Smith 1968). This method optimizes the zero levels so that the variance of the squared magnitude of the magnetic field is minimized. Rosenberg (1971) provides a detailed derivation of this technique. The Davis–Smith equation (22) was not published until Belcher (1973) developed his own method and compared it with the Davis–Smith method. Below we give an alternative derivation of the Davis–Smith method and discuss the variant of Belcher (1973), which gives greater insight into the methodology. The Belcher method optimizes the zero levels so that the maximum variance vector is orthogonal to the background field. The third method (Hedgecock 1975) is based on the assumption that averaged over a suitable time interval, there should be no correlation between changes in the field magnitude and changes in the inclination of the field to any one of the three component axes.

All three methods must be applied with some caution because the assumptions, on which each particular method is based, might not always be true. Their results stand and fall with the appropriate selection criteria for data intervals. The Davis–Smith method has no published selection criteria. Davis and Smith selected data intervals by eye (Belcher 1973). Belcher and Hedgecock published rather loose selection criteria that require long intervals (a few days to weeks) of input data.

We have modified the Davis–Smith method to determine magnetometer zero levels on much shorter time scales than previously possible. While this can be useful for all missions,

it is particularly useful when the spacecraft spends most of the time inside a magnetosphere and only occasionally enters the interplanetary magnetic field. The magnetic field is usually observed close to the bow shock and in many cases highly disturbed by non-Alfvénic upstream waves, or the spacecraft might observe the interplanetary field only because of very unusual solar wind conditions that have higher than average dynamic pressure values. Our revised method can also be used for missions that require the adjustment of zero levels at more frequent intervals than a few days as required for the published selection criteria of Belcher and of Hedgecock. Such missions may not have had an appropriate magnetic cleanliness program and therefore the magnetic field at the location of the magnetometer is heavily disturbed by the spacecraft's own time-varying magnetic field, or they may experience diurnal variations due to a changing spacecraft or sensor fields as the solar illumination or spacecraft temperature varies with orientation or the orbital position.

For convenience of the reader, below we review all three methods. This review gives us further insight into the differences between the three techniques and serves to illuminate the improvements we have made. We first discuss the Belcher and the Hedgecock methods.

1.1. Belcher's method

This method is based on the assumption that the fluctuations of the solar wind are predominantly transverse to the background field (1). It optimizes the zero levels so that the maximum variance vector (Sonnerup and Cahill 1967) is orthogonal to the background field (2). Angular brackets denote averages:

$$\delta \vec{B}_{\parallel} = \delta \vec{B} \cdot \frac{\langle \vec{B}_A \rangle}{|\langle \vec{B}_A \rangle|} \approx 0, \quad (1)$$

where $\delta \vec{B}$ is the unit vector in the maximum variance direction, $\delta \vec{B}_{\parallel}$ is the part of $\delta \vec{B}$ in the direction of the background field and \vec{B}_A is the actual background field vector:

$$\delta \vec{B}_{\parallel} \equiv 0. \quad (2)$$

Assuming that the measured field \vec{B}_M consists of the actual field \vec{B}_A plus a constant offset vector \vec{O} , we obtain

$$\delta \vec{B} \cdot \langle \vec{B}_M \rangle = \delta \vec{B} \cdot \vec{O} + \delta \vec{B} \cdot \langle \vec{B}_A \rangle, \quad (3)$$

writing the sum over n data windows (angular brackets denote averages over single data windows)

$$D = \sum_{i=1}^n (\delta \vec{B}^i \cdot \langle \vec{B}_A^i \rangle)^2 = \sum_{i=1}^n [\delta \vec{B}^i \cdot ((\vec{B}_M^i) - \vec{O})]^2, \quad (4)$$

and using $\frac{dD}{d\vec{O}} = 0$, we obtain Belcher's matrix equation

$$\sum_{i=1}^n T^i \cdot \vec{O} = \sum_{i=1}^n T^i \langle \vec{B}_M^i \rangle, \quad (5)$$

where i is the index of the data window, T^i is the outer product of $\delta \vec{B}^i$ (T is a matrix) and n is the number of data windows.

The matrix on the left-hand side of (5) is singular for $n = 1$, but (5) can still be used by selecting several data windows and solving the system of equations by using a least squares approach. Belcher's method has two selection criteria

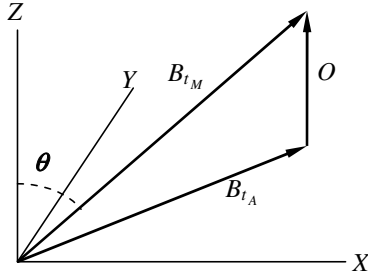


Figure 1. Relationship between the actual field magnitude B_{t_A} , the measured field magnitude B_{t_M} and the offset O .

that need to be applied to each data window. The method requires the precise knowledge of the maximum variance direction, and therefore one of his selection criteria is $\lambda_3/\lambda_1 \leq 0.1$, where λ_1 , λ_2 and λ_3 are the eigenvalues (in descending magnitude) of the same covariance matrix that was used to find the maximum variance direction (Sonnerup and Cahill 1967). His other selection criterion requires the sum of the eigenvalues to be several times above the noise level. For more detailed information, see Belcher (1973).

1.2. Hedgecock method

This method is based on the assumption that averaged over a suitable time interval, there should be no correlation between changes in the field magnitude and changes in the inclination of the field to any one of the three coordinate axes. The word ‘changes’ refers to first differences (differences of consecutive measurements, a simple approximation to the time derivative). Figure 1 shows the relationship between the actual field magnitude B_{t_A} , the measured field magnitude B_{t_M} and the offset O . Using the law of cosines, we write

$$B_{t_A}^2 = B_{t_M}^2 + O^2 - 2B_{t_M}O \cos(\theta), \quad (6)$$

where θ is the elevation angle.

Taking B_{t_A} and O as constants, differentiating and collecting terms, we obtain

$$dB_{t_M} = \frac{O \sin \theta d\theta}{1 - \frac{O}{B_{t_M}} \cos \theta}. \quad (7)$$

Assuming that the term $\frac{O}{B_{t_M}} \cos \theta$ is small (the offset is small or the measured field is approximately normal to the Z-axis), we write

$$\Delta B_{t_M} = O \sin \theta \Delta \theta. \quad (8)$$

Since $\sin \theta$ is positive for $0 < \theta < 180^\circ$, the sign of ΔB_{t_M} relative to $\Delta \theta$ depends on the sign of O . The covariance $C_{(O)}$ between ΔB_{t_M} and $\Delta \theta$ changes sign as O crosses through zero ($C_{(O)} = -C_{(-O)}$ and $C_{(O)} = 0$). Writing the equation

$$C_{(O_k)} = \frac{\sum_{j=1}^N \Delta B_{t_M(O_k)_j} \Delta \theta_{(O_k)_j}}{N-1} - \frac{\sum_{j=1}^N \Delta B_{t_M(O_k)_j} \sum_{j=1}^N \Delta \theta_{(O_k)_j}}{N(N-1)}, \quad (9)$$

where $\Delta B_{t_M(O_k)_j}$ is the difference between two consecutive measured field values at the k th iteration, $\Delta \theta_{(O_k)_j}$ is the difference between two consecutive inclination angles at the k th iteration, $C_{(O_k)}$ is the covariance for the k th value of O and N is the length of the data window.

The method requires that $C_{(O_k)}$ is calculated for a range of different offsets (e.g. using 0.1 nT steps for the offsets). The offset at the zero crossing of the covariances is the desired offset. Hedgecock’s selection criteria are such that pairs of measurements are rejected if $\theta_{(O_k)}$ lies outside of the range $30 < \theta_{(O_k)} < 150$ or $\Delta B_{t_M(O_k)} > 1$ nT. For more details, see Hedgecock (1975).

1.3. Davis–Smith method

The original derivation of the Davis–Smith method was never published in a refereed journal. It is based on minimization of the variance of the squared magnitude of the magnetic field of several (n) data windows. The initially observed uncorrected variance is

$$V_i = \langle [\vec{B}_{M_i} \cdot \vec{B}_{M_i} - \langle \vec{B}_{M_i} \cdot \vec{B}_{M_i} \rangle]^2 \rangle. \quad (10a)$$

Expanding, we obtain

$$V_i = \langle (\vec{B}_{M_i} \cdot \vec{B}_{M_i})^2 - 2\langle \vec{B}_{M_i} \cdot \vec{B}_{M_i} \rangle \langle \vec{B}_{M_i} \cdot \vec{B}_{M_i} \rangle + \langle \vec{B}_{M_i} \cdot \vec{B}_{M_i} \rangle^2 \rangle, \quad (10b)$$

which reduces to

$$V_i = \langle (\vec{B}_{M_i} \cdot \vec{B}_{M_i})^2 \rangle - \langle \vec{B}_{M_i} \cdot \vec{B}_{M_i} \rangle^2. \quad (10c)$$

If we correct the magnetic field measurement by subtracting an offset vector \vec{O}_i , the variance of the correction becomes

$$V_i^c = \langle [(\vec{B}_{M_i} - \vec{O}_i) \cdot (\vec{B}_{M_i} - \vec{O}_i)]^2 \rangle - \langle (\vec{B}_{M_i} - \vec{O}_i) \cdot (\vec{B}_{M_i} - \vec{O}_i) \rangle^2. \quad (11a)$$

Expanding, we obtain

$$V_i^c = \langle B_{M_i}^4 - 4B_{M_i}^2 (\vec{O}_i \cdot \vec{B}_{M_i}) - 4O_i^2 (\vec{O}_i \cdot \vec{B}_{M_i}) + 4\vec{O}_i (\vec{B}_{M_i} \vec{B}_{M_i}) \vec{O}_i + O_i^4 + 2B_{M_i}^2 O_i^2 \rangle - \langle B_{M_i}^2 \rangle^2 + 4\langle \vec{O}_i \cdot \vec{B}_{M_i} \rangle \langle B_{M_i}^2 \rangle + 4\langle O_i^2 \rangle \langle \vec{O}_i \cdot \vec{B}_{M_i} \rangle - 4\langle \vec{O}_i \cdot \vec{B}_{M_i} \rangle \langle \vec{O}_i \cdot \vec{B}_{M_i} \rangle - \langle O_i^2 \rangle^2 - 2O_i^2 \langle B_{M_i}^2 \rangle, \quad (11b)$$

which reduces to

$$V_i^c = \langle B_{M_i}^4 \rangle - \langle B_{M_i}^2 \rangle^2 + 4\vec{O}_i \langle \vec{B}_{M_i} \cdot \vec{B}_{M_i} \rangle \vec{O}_i - 4\langle \vec{O}_i \cdot \vec{B}_{M_i} \rangle \langle \vec{O}_i \cdot \vec{B}_{M_i} \rangle - 4\langle B_{M_i}^2 \rangle (\vec{O}_i \cdot \vec{B}_{M_i}) + 4\langle B_{M_i}^2 \rangle \langle \vec{O}_i \cdot \vec{B}_{M_i} \rangle, \quad (11c)$$

where V_i is the variance of the squared field magnitude of the data window i , V_i^c is the variance after offset adjustment, \vec{B}_{M_i} are the measured magnetic field vectors of the data window i and \vec{O}_i is the offset vector of the data window i .

Let

$$Q_i = \langle B_{M_i}^4 \rangle - \langle B_{M_i}^2 \rangle^2 \quad \text{scalar} \quad (12)$$

$$W_i = \langle B_{M_i}^2 \vec{B}_{M_i} \rangle - \langle B_{M_i}^2 \rangle \langle \vec{B}_{M_i} \rangle \quad \text{vector} \quad (13)$$

$$D_i = \langle \vec{B}_{M_i} \vec{B}_{M_i} \rangle - \langle \vec{B}_{M_i} \rangle \langle \vec{B}_{M_i} \rangle \quad \text{dyadic (covariance matrix)}. \quad (14)$$

We note that these values are all constants depending only on the measured values \vec{B}_M .

Then,

$$V_i^c = Q_i + 4\vec{O}_i(D_i)\vec{O}_i - 4\vec{O}_i\vec{W}_i. \quad (15)$$

Minimization of V_i^c by differentiating with respect to \vec{O}_i gives

$$\vec{O}_i(D_i) = \frac{\vec{W}_i}{2}, \quad (16)$$

which is the Davis–Smith equation. For a mathematically less abstract version of this equation, see (22). A combination of all data windows leads to

$$\sum_{i=1}^n D_i \cdot \vec{O} = \frac{1}{2} \sum_{i=1}^n \vec{W}_i, \quad (17)$$

where n is the number of data windows and \vec{O} is the offset for all combined data windows.

2. Mathematical insights into the Davis–Smith equation

2.1. Derivation of the Davis–Smith equation using correlations

It is instructive to show that if one starts with the assumption that $|B_M|^2$ is uncorrelated with the variance along any one of the three component axes, we obtain the same result.

Recall that the sample covariance can be written in three different ways:

$$S_{xy} = \frac{1}{N-1} \sum_{j=1}^N (x_j - \langle x \rangle)(y_j - \langle y \rangle) \quad (18a)$$

$$= \sum_{j=1}^N \frac{x_j y_j}{N-1} - \frac{\sum_{j=1}^N x_j \sum_{j=1}^N y_j}{N(N-1)} \quad (18b)$$

$$= \langle xy \rangle - \langle x \rangle \langle y \rangle. \quad (18c)$$

We note that adding an offset to any or all three component axes will not alter their mutual covariances. Setting S_{xy} to zero using (18c), our assumption of the lack of correlation between $|B_A|^2$ and each of the three component axes implies that

$$\begin{aligned} \langle B_1 |B_A|^2 \rangle &= \langle B_1 \rangle \langle |B_A|^2 \rangle \\ \langle B_2 |B_A|^2 \rangle &= \langle B_2 \rangle \langle |B_A|^2 \rangle \\ \langle B_3 |B_A|^2 \rangle &= \langle B_3 \rangle \langle |B_A|^2 \rangle, \end{aligned} \quad (19)$$

where $|B_A|^2$ is the actual squared magnitude of the field.

Introducing offsets O_1 , O_2 and O_3 along each of the sensors,

$$|B_M|^2 = |B_A|^2 + 2O_1 B_1 + 2O_2 B_2 + 2O_3 B_3 + O_1^2 + O_2^2 + O_3^2. \quad (20)$$

Rewriting (19) we obtain

$$\begin{aligned} &\langle B_1(|B_M|^2 - 2O_1 B_1 - 2O_2 B_2 - 2O_3 B_3) \rangle \\ &= \langle B_1 \rangle (\langle |B_M|^2 \rangle - 2O_1 \langle B_1 \rangle - 2O_2 \langle B_2 \rangle - 2O_3 \langle B_3 \rangle) \\ &\langle B_2(|B_M|^2 - 2O_1 B_1 - 2O_2 B_2 - 2O_3 B_3) \rangle \\ &= \langle B_2 \rangle (\langle |B_M|^2 \rangle - 2O_1 \langle B_1 \rangle - 2O_2 \langle B_2 \rangle - 2O_3 \langle B_3 \rangle) \\ &\langle B_3(|B_M|^2 - 2O_1 B_1 - 2O_2 B_2 - 2O_3 B_3) \rangle \\ &= \langle B_3 \rangle (\langle |B_M|^2 \rangle - 2O_1 \langle B_1 \rangle - 2O_2 \langle B_2 \rangle - 2O_3 \langle B_3 \rangle). \end{aligned} \quad (21)$$

From (18a) it is easy to see that since O_1^2 , O_2^2 and O_3^2 do not change in time, they do not change the covariance and for that reason can be omitted from (21).

After bringing all offsets to one side, one can write the equation as

$$\begin{aligned} &\begin{pmatrix} \langle B_1^2 \rangle - \langle B_1 \rangle^2 & \langle B_1 B_2 \rangle - \langle B_1 \rangle \langle B_2 \rangle & \langle B_1 B_3 \rangle - \langle B_1 \rangle \langle B_3 \rangle \\ \langle B_2 B_1 \rangle - \langle B_2 \rangle \langle B_1 \rangle & \langle B_2^2 \rangle - \langle B_2 \rangle^2 & \langle B_2 B_3 \rangle - \langle B_2 \rangle \langle B_3 \rangle \\ \langle B_3 B_1 \rangle - \langle B_3 \rangle \langle B_1 \rangle & \langle B_3 B_2 \rangle - \langle B_3 \rangle \langle B_2 \rangle & \langle B_3^2 \rangle - \langle B_3 \rangle^2 \end{pmatrix} \begin{pmatrix} O_1 \\ O_2 \\ O_3 \end{pmatrix} \\ &= \frac{1}{2} \begin{pmatrix} \langle B_1 |B_M|^2 \rangle - \langle B_1 \rangle \langle |B_M|^2 \rangle \\ \langle B_2 |B_M|^2 \rangle - \langle B_2 \rangle \langle |B_M|^2 \rangle \\ \langle B_3 |B_M|^2 \rangle - \langle B_3 \rangle \langle |B_M|^2 \rangle \end{pmatrix}. \end{aligned} \quad (22)$$

Equation (22) is the same as (16). This demonstrates that the Davis–Smith method is also a correlation technique. The matrix on the left-hand side of (22) is the covariance matrix that is independent of the offset.

2.2. Davis–Smith equation for first differences

It is similarly instructive to derive the Davis–Smith method for first differences. Equation (23) is the time derivative of (20):

$$\frac{d|B_M|^2}{dt} = \frac{d|B_A|^2}{dt} + 2O_1 \frac{dB_1}{dt} + 2O_2 \frac{dB_2}{dt} + 2O_3 \frac{dB_3}{dt}. \quad (23)$$

In (23), the terms $2O_1$, $2O_2$ and $2O_3$ are still present and $\frac{d|B_A|^2}{dt}$ is constant for a pure rotation as well as a linear change of the field magnitude. Thus making the covariance between $\frac{d|B_M|^2}{dt}$ and $\frac{dB_1}{dt}$, $\frac{dB_2}{dt}$ and $\frac{dB_3}{dt}$ zero yields $2O_1$, $2O_2$ and $2O_3$. Formulating equation (21) for first differences yields

$$\begin{aligned} &\langle \Delta B_1 (\Delta |B_M|^2 - 2O_1 \Delta B_1 - 2O_2 \Delta B_2 - 2O_3 \Delta B_3) \rangle \\ &= \langle \Delta B_1 \rangle (\langle \Delta |B_M|^2 \rangle - 2O_1 \langle \Delta B_1 \rangle - 2O_2 \langle \Delta B_2 \rangle \\ &\quad - 2O_3 \langle \Delta B_3 \rangle) \\ &\langle \Delta B_2 (\Delta |B_M|^2 - 2O_1 \Delta B_1 - 2O_2 \Delta B_2 - 2O_3 \Delta B_3) \rangle \\ &= \langle \Delta B_2 \rangle (\langle \Delta |B_M|^2 \rangle - 2O_1 \langle \Delta B_1 \rangle - 2O_2 \langle \Delta B_2 \rangle \\ &\quad - 2O_3 \langle \Delta B_3 \rangle) \\ &\langle \Delta B_3 (\Delta |B_M|^2 - 2O_1 \Delta B_1 - 2O_2 \Delta B_2 - 2O_3 \Delta B_3) \rangle \\ &= \langle \Delta B_3 \rangle (\langle \Delta |B_M|^2 \rangle - 2O_1 \langle \Delta B_1 \rangle - 2O_2 \langle \Delta B_2 \rangle \\ &\quad - 2O_3 \langle \Delta B_3 \rangle). \end{aligned} \quad (24)$$

Bringing all offsets to one side yields the same equations as (16) and (22) but for first differences as input. This means that equations (16) and (22) can be used for both magnetic field data and first differences of magnetic field data. At this point, we would like to mention that there is another computationally less expensive solution to (24). Assuming that $\frac{d|B_A|^2}{dt}$ is zero (which is true for a pure rotation), the offsets can be directly brought to one side which leads to a simpler equation:

$$(\Delta B_1 \quad \Delta B_2 \quad \Delta B_3) \begin{pmatrix} O_1 \\ O_2 \\ O_3 \end{pmatrix} = \frac{1}{2} \Delta |B_M|^2. \quad (25)$$

Interestingly enough, for first differences, equation (25) is identical to equation (16) in Acuña (2002) even though his equation was derived completely differently.

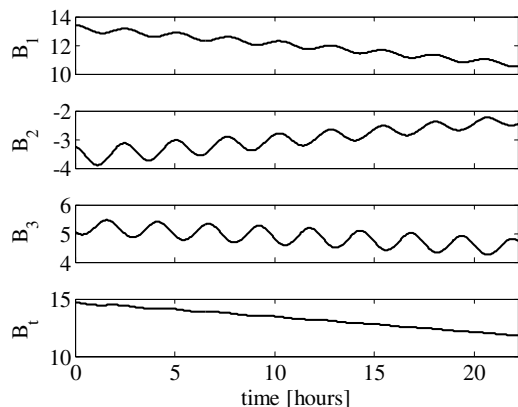


Figure 2. Artificially generated data that contain pure rotations while the field strength B_t is smoothly and slightly nonlinearly decreasing.

2.3. Davis–Smith equation for filtered data

It is again instructive to derive the Davis–Smith method for filtered data (see equation (26))

$$F(|B_M|^2) \approx F(|B_A|^2) + 2O_1 F(B_1) + 2O_2 F(B_2) + 2O_3 F(B_3), \quad (26)$$

where $F()$ denotes the filter function.

Similarly, as for first differences, equation (21) can also be formulated for filtered data. Equation (25) can also be used for filtered data if the filter removes the dc components and low frequencies. The cut-off frequency needs to be higher than one divided by the length of the data window.

Using filters makes it possible to filter out slow changes in the field magnitude. Figure 2 shows an example of artificially generated data by using simple mathematical functions. The data set contains pure rotations around two non-parallel axes, while the magnetic field strength smoothly decreases (slightly nonlinear). We added a 2 nT offset in each component leading to small ripples in the field magnitude B_t . We then applied the Davis–Smith equation to this data set in three different ways. First, we used the unfiltered data which returned $O_1 = 11.92$ nT, $O_2 = -3.08$ nT and $O_3 = 4.80$ nT. Second, we used first differences which returned $O_1 = 1.58$ nT, $O_2 = 2.21$ nT and $O_3 = 1.88$ nT which is in this case a great improvement (due to the almost linear decrease of the field). Third, we applied a high-pass filter to remove the decrease of the total field while keeping the ripples unchanged which yielded the correct $O_1 = 2.00$ nT, $O_2 = 2.00$ nT and $O_3 = 2.00$ nT. Additionally, we calculated the offset using (25) which yielded $O_1 = 11.83$ nT, $O_2 = -2.87$ nT, $O_3 = 4.88$ nT. This result is, in this case, not as good as using the full Davis–Smith equation and first differences as input (see above). The assumption that $\frac{d|B_A|^2}{dt}$ is equal to zero is violated due to the continuous decrease of the field magnitude.

At this point, we should discuss a postulate stated by Hedgecock: ‘A possible criticism of the above two methods (methods by Davis–Smith and Belcher) is that they tend to maximize the Alfvénic character (i.e. field magnitude conserving) of the selected fraction of observations even

though there is no *a priori* reason why the disturbances should be strictly Alfvénic in nature. In the following we present a technique for zero level determination which does not suffer from this objection . . .’. Also the fact that Hedgecock correlates the field magnitude with an inclination angle rather than the component itself does not make a significant difference. The component and the inclination angle are directly related. However, this does make it impossible to find a simple analytical solution. First differences are often very small quantities, and small compressional disturbances can have an undesired influence on the outcome of zero level calculations. In general, for relatively long intervals (as used by Belcher and Hedgecock), there is no significant difference if one uses first differences or not. For shorter intervals, however, there is often a difference (see the above example).

Major advantages can be achieved when a filter is applied. This makes it possible to filter out disturbances such as slow changes in the field magnitude or stray fields caused by the spacecraft. With the exception of shocks, fast magnetosonic waves tend to smooth out compressional disturbances in the solar wind while Alfvénic structures persist. For example, a high-pass filter (with a cutoff frequency of a few mHz) does not reduce the variance of the magnetic field measurements as drastically as taking the derivative. This conserves a larger range of input values. Correlations are very sensitive to phase shifts; therefore, it is crucial that the filter is a zero-phase filter. Additionally, the filter should conserve the amplitude of the pass-band and thus for our work we use Butterworth-type filters. The Davis–Smith equation (22) can handle all types of filters (high-pass, low-pass, band-pass and band-stop), no matter how many of the dc components of the data are preserved.

For a spinning spacecraft with no ac fields at the spin frequency, say due to asymmetries in the solar panel configuration, only the offset along the spin axis needs to be calculated and the Davis–Smith equation can be simplified to $(\langle B_3^2 \rangle - \langle B_3 \rangle^2) O_3 = \frac{1}{2} (\langle B_3 | B_M|^2 \rangle - \langle B_3 \rangle \langle |B_M|^2 \rangle)$, (27) where we assume the third component to be the spin axis.

2.4. Mathematical superiority of the Davis–Smith equation

The main advantage of the Davis–Smith equation over the equations by Belcher and Hedgecock is its versatility. It works for unaltered as well as for filtered data and for first differences. Another advantage over the method by Hedgecock is that it provides analytical solutions for all three component axes if needed and therefore omit the need for iterations through various offset values. A third major advantage over Belcher’s method is that the Davis–Smith equation is not singular if applied to just one data window. This is critical for establishing sophisticated selection criteria for data windows (see section 3). Belcher’s matrix is singular for one data window because two of its eigenvalues are zero. This means that each data window only provides information along one direction, whereas the Davis–Smith equation is capable of providing information along all three component axes of the principal coordinate system of each data window. In other words, Belcher’s equation does not use all available information.

3. Selection criteria for the Davis–Smith method

After having established the mathematical superiority of the Davis–Smith equation, we need to find the optimum selection criteria. We start with a discussion of previously published selection criteria by Belcher and Hedgecock. As mentioned above, Belcher uses the criterion $\lambda_3/\lambda_1 \leq 0.1$. The eigenvalues of the covariance matrix are a measure of the variance along the principal axes. As mentioned in the previous section, Belcher’s equation allows each data window only to contain information along one direction (the maximum variance direction). The ratio λ_3/λ_1 is therefore a suitable criterion for his method, even though occasionally this leads to the selection of data windows that contain pure compressions. This can happen (but not necessarily) when both λ_3 and λ_2 are small compared to λ_1 . Hedgecock’s selection criteria are dependent on the zero level. This means that for each iteration, the selected data set changes. This can lead to multiple zero crossings of the calculated set of covariances, thus failing to provide a unique solution. The Davis–Smith equation can handle information (variance) along all the three axes of the principal coordinate system; therefore, all three eigenvalues of each data window should be as large as possible (additional criteria needed, see below).

Figure 3(a) shows an example of STEREO-A magnetic field data (starting at 26 March 2007, 13:40:51) displayed in spacecraft coordinates. Figure 3(b) contains the same data as figure 3(a) but rotated into minimum variance coordinates to show that the variance is present along all three principal axes. The third panel of figure 3(b) contains the component with the smallest variance. For a pure rotation of the interplanetary magnetic field, a plot of the squared field magnitude versus either one of its component axes should look like a straight line with zero gradient (assuming all zero levels are correct). Figure 3(c) shows slopes before and after the correct zero levels have been applied. The gray slopes are nonlinear because the zero levels are incorrect for all three components; the black horizontal lines are close to being linear due to the presence of rotations around various non-parallel axes and corrected zero levels. For the case that there are rotations and that the zero levels are correct for two axes but incorrect for one axis, the slope is still linear and its gradient is equal to twice the required offset correction (see black points in figure 3(d)). If we introduce an incorrect zero level in another component, the slope becomes nonlinear (see gray points in figure 3(d)). After we have applied the correct zero levels to the data in figure 3(a), we get an extremely flat field magnitude confirming that the variances along all three components are mostly rotational (see figure 3(e)).

In the case of pure compressions along one component axis (while the other two components stay constant), the plot of the squared magnitude versus that particular component resembles a parabola (see figure 4). In reality, there are neither pure rotations nor pure compressions; the field behavior is somewhat in between. Our task is to separate rotations that are pure enough to give reliable offset estimates from those that are too heavily disturbed by compressions. Let us take a closer look at the second case, where we have pure

Table 1. Three examples of empirically determined criteria used in calculations. STEREO is a dual-spacecraft mission with three-axis stabilization where the zero levels of all three component axes need to be calibrated. THEMIS is a five-spacecraft mission with spin stabilization where only the zero level of the component that lies along the spin axis needs to be calculated. Venus Express (VEX) is a three-axis stabilized spacecraft.

Mission	STEREO	THEMIS	VEX
Data resolution	1 s	3 s	1 s
Selection			
<i>mcs</i>	0.25 nT	0.25 nT	0.3 nT
ε_1	1 * <i>mcs</i>	1 * <i>mcs</i>	1 * <i>mcs</i>
ε_2	0.5	0.5	0.5
ε_3	1 * <i>mcs</i>	1 * <i>mcs</i>	1 * <i>mcs</i>
c_1	1.25	1.25	1.25
Windowing			
<i>wp₁</i>	320 s	300 s	320 s
<i>wp₂</i>	3600 s	3000 s	3600 s
<i>wp₃</i>	20%	5%	20%
<i>s</i>	8 s	3 s	8 s
Inversion			
c_2	1.5	1.5	2.0
<i>npts</i>	1000	300	1000
<i>ni</i>	10	10	10
Monte Carlo			
<i>nmc</i>	300	300	300
c_3	2.0	2.0	3.0

compressions, along one component axis. If one naively makes the correlation between the field magnitude and that component goes to zero by changing the zero level, the average of that component will be removed because the derivative of x^2 (a parabola) is $2x$. For this reason, the Davis–Smith method tends to remove the averages of the component axes if applied to data with too much compressional content.

For intervals that have a small variance in the component axes, it is difficult to decide whether a slope is truly linear. The data points from the data window, once corrected, should lie on a straight line with zero gradient. There is a certain minimal required variance that allows us to find linear slopes. For the description of most of our criteria that we apply for finding zero levels, we need to introduce the term *mcs* which is the minimal compressional standard deviation that we want to resolve.

3.1. First selection criterion

In order to solve for all three zero levels, significant rotations around various non-parallel axes are required. As stated above, we combine many data windows and perform a single large inversion. Each data window is required to contain fluctuations that lie at least within a single plane. A combination of such data windows can still contain fluctuations that lie inside multiple non-parallel planes. Thus, our first criterion requires that the square root of the second eigenvalue of the covariance matrix is greater than a certain threshold, namely $\sqrt{\lambda_2} > \varepsilon_1$. In our work, we usually set $\varepsilon_1 = mcs$ (see table 1). For a spinning spacecraft, the criterion changes to $\text{std}(B_3) > \varepsilon_1$ (where we assume the third axis to be the spin axis).

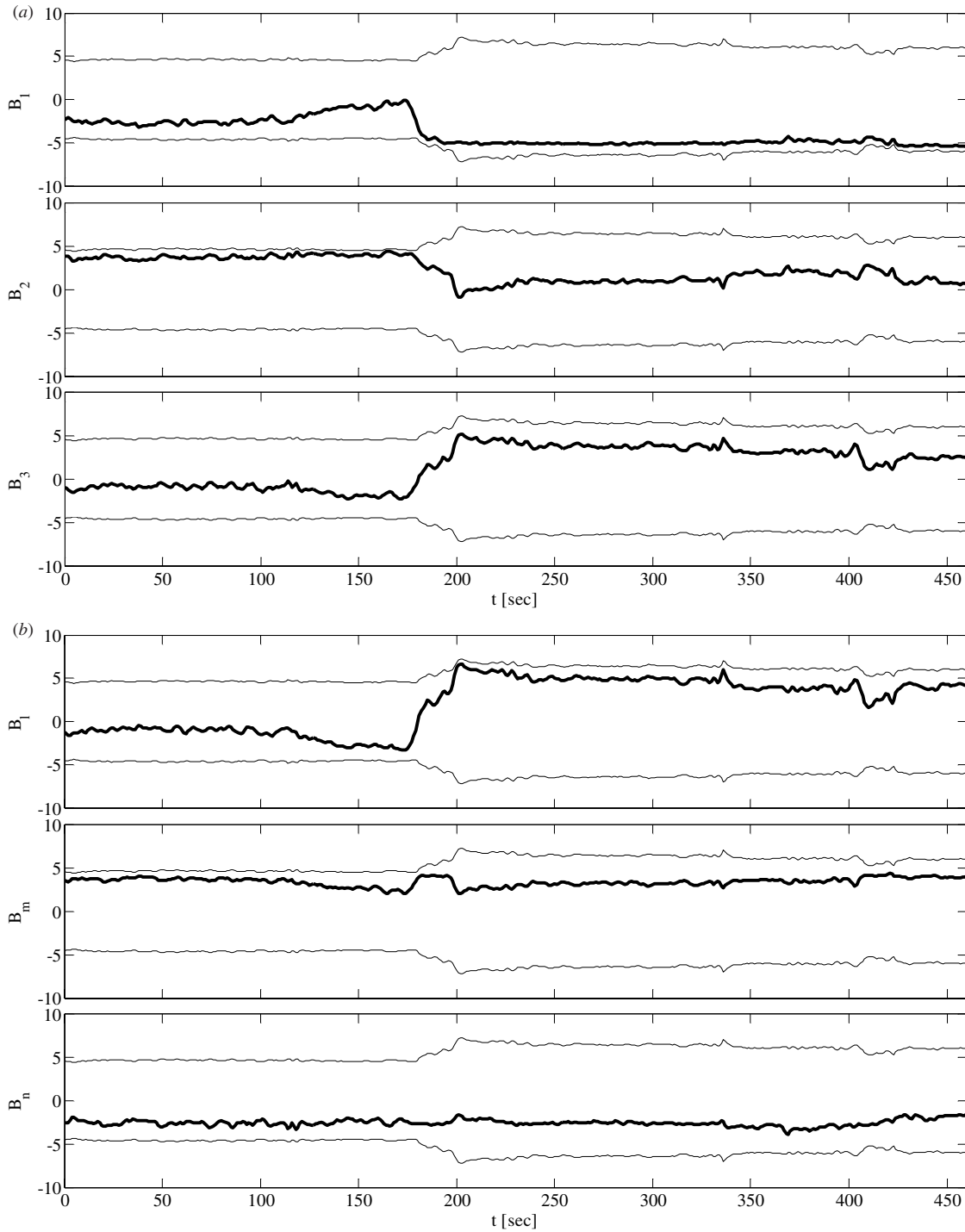


Figure 3. (a) A short example of STEREO-A data in the spacecraft coordinate system. The thin black lines are the magnetic field magnitude and its negative value plotted on the same scale to illustrate when the field was largely along or orthogonal to the sensors. The zero levels are incorrect. $O_1 = 1$ nT, $O_2 = -1$ nT and $O_3 = 2$ nT. (b) Same data as in figure 3(a), but rotated into the minimum variance coordinate system to show that there is variance along all the three axes of the principal coordinate system. The square roots of the eigenvalues (same as standard deviations in the minimum variance coordinate system) are given in a descending order: 3.03 nT, 0.48 nT and 0.38 nT. (c) Squared magnitude (B_i^2) versus component plots. The averages have been subtracted to center the plots at the origin. Gray: before zero levels have been applied. Black: after zero levels have been applied. (d) Black: O_1 is incorrect, whereas O_2 and O_3 are correct. This causes a slope with gradient of $2O_1$ that is close to linear. $O_1 = 1$ nT. Gray: O_1 and O_3 are incorrect, whereas O_2 is correct. The introduction of an offset in another component causes a highly nonlinear slope. $O_1 = 1$ nT and $O_3 = 2$ nT. (e) The data in figure 3(a) after the zero levels have been applied. The thin black traces are the mirrored field magnitude. The variance of the squared magnitude (thin black traces) has been greatly reduced compared to figure 3(a), confirming that the variances in the component axes are mostly rotational.

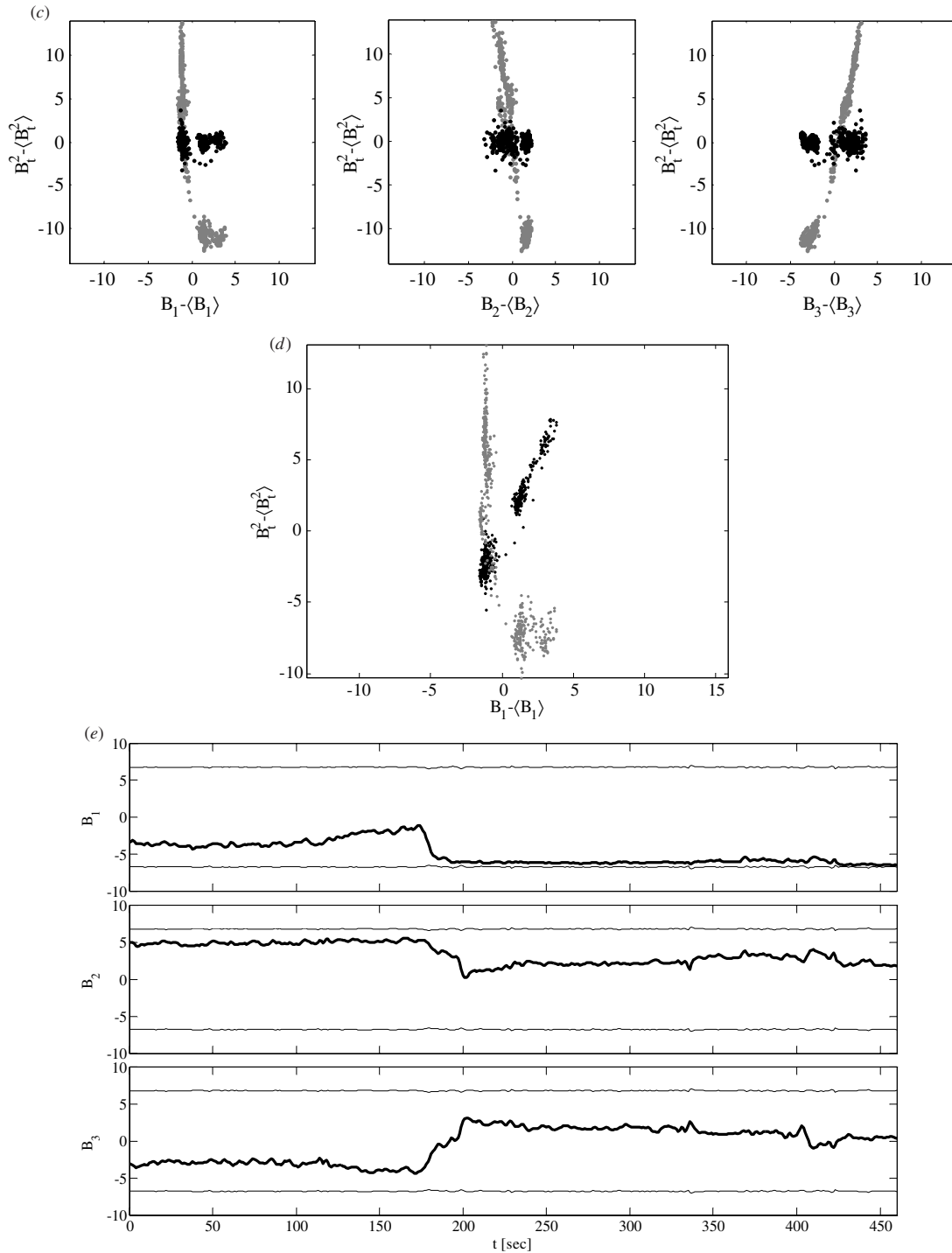


Figure 3. (Continued.)

3.2. Second selection criterion

The second selection criterion describes how ‘clean’ particular rotations within a certain data window are. By computing the ratio $\frac{\lambda_2}{\text{std}(|B_A|^2)} > \varepsilon_2$, we can get a measure of this property. We normally choose $\varepsilon_2 = 0.2$ to 0.5 . This selection criterion is applied after the zero levels have been calculated using

equations (22) or (27) because $\text{std}(|B_M|^2)$ changes toward $\text{std}(|B_A|^2)$ when the zero levels change toward their correct values (see the black curves in figure 3(c) or compare the thin black traces in figure 3(a) with the corresponding traces in figure 3(e)). For a spinning spacecraft, we replace λ_2 by $\text{var}(B_3)$ (where we assume the third axis to be the spin axis).

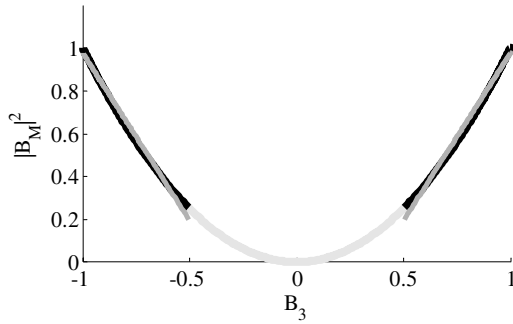


Figure 4. A theoretical example of a pure compression. Magnitude squared versus the component along which there is a pure compression. For this example, we chose the other two components (B_1 and B_2) to be zero. Black: upper and lower quartile of B_3 . The straight slopes represent twice the offsets that would be calculated using only the upper and lower quartile. The difference of these offsets is used for our third selection criterion (the linearity criterion).

3.3. Third selection criterion

Our third selection criterion decides whether a particular slope exhibits sufficient linearity with a gradient of zero. Since this selection criterion requires much computational effort, we only apply it if the first two selection criteria are fulfilled. This selection criterion is applied after the zero levels have been calculated (using equations (22) or (27)) and subtracted from the data. We sort the magnetic field measurements of a data window, in three different ways, according to B_1 , B_2 and B_3 and we always exchange the values of $|B_A|^2$ according to the corresponding sorting procedure. After the sorts have been performed, we have B_1 , B_2 and B_3 in an ascending order and their corresponding values of $|B_A|^2$ ($|B_A|^2$ in three different sequences). Then we start with sorted B_1 and take the first quarter of values and calculate the offset O_{11} using the Davis–Smith equation (27) that solves for only one component. Similarly, we calculate the offset O_{12} for the second quarter of values and so on. Then we search the maximum and minimum values of the four calculated offsets and use the criterion $\text{abs}(O_{1\max} - O_{1\min}) < \varepsilon_3$ (see figure 4). For a long data interval with pure compressions having a standard deviation of mcs , $\text{abs}(O_{1\max} - O_{1\min})$ should be $\sim 2 mcs$ (if the sum of the squares of the other two components is constant). To be conservative, we use $\varepsilon_3 = mcs$ as our threshold. We do the same for the other two component axes. In the case of a spinning spacecraft, only one component has to be taken into account.

3.3.1. Making the third selection criterion robust. It is likely that not all three component axes fulfill the third selection criterion for the same data window. A particular data window can still be used if at least one component passes the selection criteria. In this case, the other two component axes that do not pass the selection criteria should not have a significant influence on the calculation of the offset of the component that passes. The component axes influence one another via the off-diagonal terms (covariances) in (22). We need to prevent the off-diagonal terms from dominating the matrix in such a

way that the offsets of the components that pass cannot be determined correctly. As an example, we assume that only the first component passes. We then check the covariances of the other components in the following way:

$$\langle B_1^2 \rangle - \langle B_1 \rangle^2 > \text{abs}(O_{2\max} - O_{2\min})\text{abs}(\langle B_1 B_2 \rangle - \langle B_1 \rangle \langle B_2 \rangle) \\ + \text{abs}(O_{3\max} - O_{3\min})\text{abs}(\langle B_1 B_3 \rangle - \langle B_1 \rangle \langle B_3 \rangle),$$

where we use $\text{abs}(O_{2\max} - O_{2\min})$ and $\text{abs}(O_{3\max} - O_{3\min})$ as estimates of how much the offsets O_2 and O_3 are being compromised. Now let us assume that the first two components pass. Then we check against the third component by doing two checks:

$$\langle B_1^2 \rangle - \langle B_1 \rangle^2 > \text{abs}(O_{3\max} - O_{3\min})\text{abs}(\langle B_1 B_3 \rangle - \langle B_1 \rangle \langle B_3 \rangle) \\ \langle B_2^2 \rangle - \langle B_2 \rangle^2 > \text{abs}(O_{3\max} - O_{3\min})\text{abs}(\langle B_2 B_3 \rangle - \langle B_2 \rangle \langle B_3 \rangle).$$

Similarly, we do these checks for all other possible cases.

If one looks at just one data window, the checks of the covariances are rather loose because the estimated errors used for cross checking might not always be accurate, but statistically a large error of the offset of another component combined with a large covariance reduces the chance of correct offset estimate of the component of interest. At this point, we are just trying to avoid large outliers. In section 5, we show how we combine all data windows. When we combine all data windows, we assume that the influence of the components that did not pass cancels each other out to a large extent. For a spinning spacecraft, the covariances do not need to be taken into account.

After we have applied all of our selection criteria, it is still possible to get outliers. We expect that the offsets that pass the third selection criterion are correct to a certain extent. We calculate the standard deviation of all offsets that pass our tests. We throw out offsets that have a larger difference from the median than a multiple c_1 of the standard deviation. For our work, we usually use $c_1 = 1.25$. For a spinning spacecraft, only one component needs to be taken into consideration.

The value that we set for mcs is dependent on the distance from the Sun as well as noise in the data and disturbances introduced by the spacecraft's magnetic field and the chosen high-pass filter. Table 1 shows three example sets of criteria that we used in our work. The value for each criterion has been determined empirically. In general, we use the same values for filtered and unfiltered data. We chose our selection criteria in such a way that in general, mcs is the only parameter that needs to be changed according to the distance from the Sun.

4. Windowing

Our method works with a data-window length that varies from about 5 min to about 1 h (parameters: wp_1 minimal data-window length, wp_2 maximal data-window length). The shift step s is constant and smaller than half of the smallest data-window length. Each data window regardless of its length is shifted with the shift step s over the whole set of input data. This means that a single data point can be part of several data windows. The variable data-window length gives us three advantages: the method scales itself toward optimal data-window length, we obtain more accurate tracking of the

beginnings and ends of pure rotations and we weigh more heavily long consistent intervals of pure rotations.

We start at the smallest data-window length (320 s) and increase the length subsequently by wp_3 per cent until we reach the largest data-window length (3600 s). For our work, we used $wp_3 = 5$ to 20%. We have used shift steps from $s = 3$ to 16 s. We combine all selected data windows regardless of their length and perform one large inversion. Variable data-window lengths greatly increase the number of data windows and thus the number of required computations. We implement our algorithm in such a way that we use cumulative sums as often as possible.

5. Combination of data windows and overall inversion

It is possible to combine all selected data windows in a very simple way which avoids large matrices. For each data window, we subtract all the averages from B_1 , B_2 , B_3 and $|B_M|^2$. Then we use the following equation to combine all the values of all data windows which is a simpler form of (22):

$$\begin{pmatrix} \langle B_1^2 \rangle & \langle B_1' B_2' \rangle & \langle B_1' B_3' \rangle \\ \langle B_2' B_1' \rangle & \langle B_2'^2 \rangle & \langle B_2' B_3' \rangle \\ \langle B_3' B_1' \rangle & \langle B_3' B_2' \rangle & \langle B_3'^2 \rangle \end{pmatrix} \begin{pmatrix} O_1 \\ O_2 \\ O_3 \end{pmatrix} = \frac{1}{2} \begin{pmatrix} \langle B_1' | B_M |^2 \rangle \\ \langle B_2' | B_M |^2 \rangle \\ \langle B_3' | B_M |^2 \rangle \end{pmatrix}. \quad (28)$$

For a spinning spacecraft, we use

$$\langle B_3'^2 \rangle O_3 = \frac{1}{2} \langle B_3' | B_M |^2 \rangle, \quad (29)$$

where B_1' , B_2' , B_3' and $|B_M|^2$ are all magnetic field values of all data windows that had the averages removed.

Even after the input has passed our selection criteria, we have to decide whether the overall inversion has produced meaningful results. We check if it contains rotations around various non-parallel axes by the requirement that the standard deviation of each component that went into the final inversion is greater than $c_2 * mcs$. If a particular component fails to meet this criterion, we do not trust the offset for that component. In our work, we have used $c_2 = 1.5$ to 2. Another criterion is the number of independent points $npts$ that went into the inversion (each measurement is counted only once even if it is part of several data windows). We have set this value to $npts = 1000$ for 1 s data. This value largely depends on the resolution of the data. The next criterion is the number of different data windows ni that went into the overall inversion. We usually set this value to 10. For a spinning spacecraft, the offset from all combined data windows can be calculated using (29).

If none of the components fulfill the criteria of the overall inversion, one could loosen criteria one, two and three so that more data windows get selected. In some cases, it is better to have more data windows that were chosen using less tight criteria than very few data windows chosen with strict criteria. In some cases, changing the cutoff frequency of the high-pass filter can produce a higher number of valid data windows.

6. Monte Carlo simulation

Once we have performed the overall inversion, we need to check if the obtained solutions are stable solutions. As a Monte Carlo simulation, we chose to use a modified version of the so-called Bootstrap method (Efron 1982). This method reduces the information content of the data set which consists of n independent measurements by randomly choosing n times a measurement out of the n measurements. This leads to a new data set that has roughly $1/e$ measurements more than once. This procedure is done a large number of times, and each time a new inversion is performed. The variance of the solutions is then used as a measure of stability. In the case of interplanetary magnetic field measurements, two consecutive measurements are generally not independent (e.g. for 1 s resolution). In order to achieve some degree of independence in our work, we used 2 min intervals instead of single points. Since we have variable window lengths, the same 2 min interval can be part of several data windows. If a particular 2 min interval did not get chosen, it was removed from all data windows. For our work, we performed 300 to 500 inversions (parameter: nmc). We decide that an offset is determined in a stable fashion if the difference between the maximum and the minimum estimates is smaller than $c_3 * mcs$. It is possible that not all three offset estimates are stable. If at least one estimate is stable, we apply the stable offset(s) to the data and repeat the overall inversion and the Monte Carlo simulation for the remaining component(s) but we leave out the data windows that fulfill the third selection criterion only for the stable component(s). This leads to a data set that was especially chosen in order to solve for the remaining component(s). If only one component remains, the algorithm is the same as for a spinning spacecraft. We use the maximum and minimum estimates to define our error bars.

If no stable solution can be found, one could try tweaking the selection criteria. For example, if the noise level of the data is rather low one could loosen the criteria that are based on eigenvalues or variance (ϵ_1 , ϵ_2 and c_3). One could also try lowering the shift step s in order to better track beginnings and ends of pure rotations or decrease the increment of the window length wp_3 from, e.g., 20% to 10%. Another possibility would be that too many compressions slipped through. In this case, increasing mcs could help in finding stable solutions.

7. Application of our algorithm to space-borne magnetometer data

Figure 5 shows an example of magnetic field data where the field magnitude is continuously declining throughout the interval. The data were measured on the three-axis stabilized STEREO-A while passing through the interior of an interplanetary coronal mass ejection (ICME). For this interval, we could only obtain zero levels by high-pass filtering the data. First differences as well as unfiltered data did not yield results because no data windows were selected by our algorithm.

Tables 2 and 3 show the results of a calibration performed with STEREO-B data for day 224 of 2007. The input parameters are given in table 1. The first run did not return a

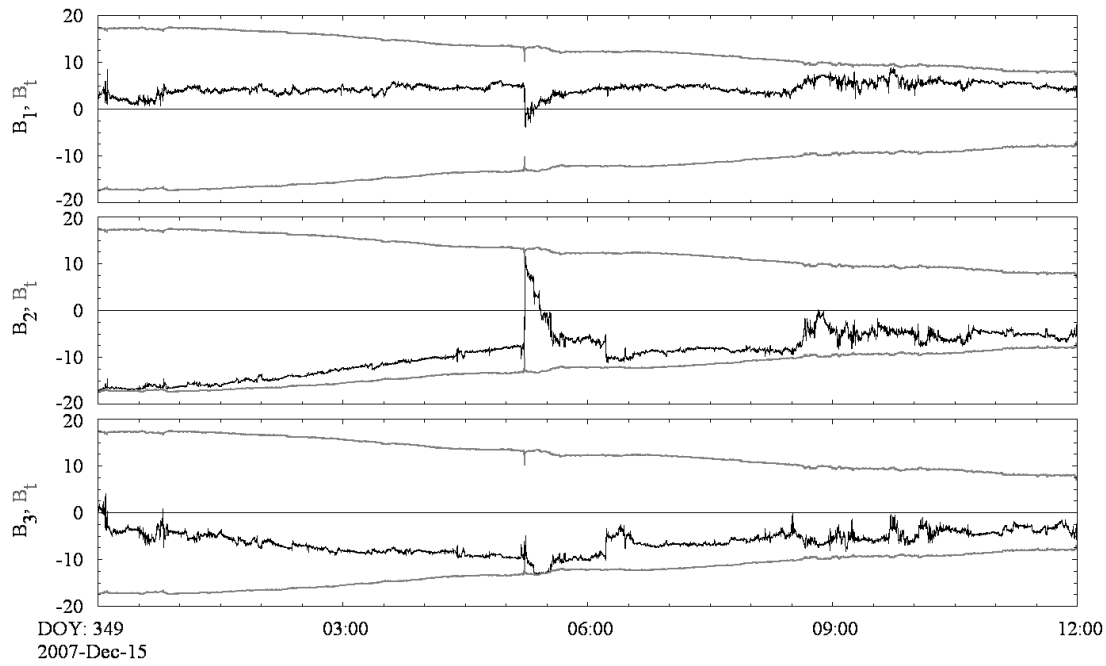


Figure 5. Magnetic field data of STEREO-A as it passes through the interior of an ICME. Shown in black are the outputs of the three magnetometer sensors at 1 s resolution. The light gray lines are the magnetic field magnitude B_t and its negative value is plotted on the same scale to illustrate when the field was largely along or orthogonal to the sensors. Zero-phase high-pass filtering is applied on these data before our zero level determination algorithm. The filter is a fourth order (eighth order when zero-phase filtering) Butterworth-type filter with a cutoff frequency of 8.9 mHz.

Table 2. Example of STEREO-B zero level calculations for day 224 of 2007. For the filtered case, the cutoff frequency of the high-pass filter is 3.3 mHz. The fields that are marked in gray represent violations of criteria which lead to the dismissal of O_1 from the filtered case and the dismissal of O_3 from both cases. The full set of selection criteria is given in table 1.

	Unfiltered input data	Filtered input data
Inversion		
Number of independent points	13 648	12727
Number of data windows	359	570
std(B_1) (nT)	1.408	0.338
std(B_2) (nT)	0.614	0.398
std(B_3) (nT)	0.555	0.185
O_1 (nT)	-43.63	-43.99
O_2 (nT)	19.92	20.10
O_3 (nT)	-37.85	-37.50
Monte Carlo simulation		
abs($O_{1min} - O_{1max}$) (nT)	0.321	-
abs($O_{2min} - O_{2max}$) (nT)	0.196	0.147
abs($O_{3min} - O_{3max}$) (nT)	0.525	-
Result		
O_1 (nT)	-43.63	-
O_2 (nT)	19.92	20.10
O_3 (nT)	-	-
Error bars		
O_{1min} to O_{1max} (nT)	-43.89 to -43.57	-
O_{2min} to O_{2max} (nT)	19.83 to 20.02	20.03 to 20.17
O_{3min} to O_{3max} (nT)	-	-
Combined result		
O_1 (nT)	-43.63	-
O_2 (nT)	20.01 (averaged)	-
Combined error bars		
O_{1min} to O_{1max} (nT)	-43.57 to -43.89	-
O_{2min} to O_{2max} (nT)	19.83 to 20.17 (worst case of both estimates)	-

Table 3. Rerun of the algorithm in order to solve for O_3 . Before we performed the rerun, we applied the corrected zero levels O_1 and O_2 as given in table 2 to the input data.

	Unfiltered input data		Filtered input data	
	Inversion			
Number of independent points	19 687	$>npts = 1000$	12879	$>npts = 1000$
Number of data windows	331	$>ni = 10$	1035	$>ni = 10$
std(B_3) (nT)	0.575	$>c_2 * mcs = 0.375$	0.373	$>c_2 * mcs = 0.375$
O_3 (nT)		-37.99		-38.07
	Monte Carlo simulation			
abs($O_{3_{\min}} - O_{3_{\max}}$) (nT)	0.17	$<c_3 * mcs = 0.5$	0.19	$<c_3 * mcs = 0.5$
	Result			
O_3 (nT)		-37.99		—
	Error bars			
$O_{3_{\min}}$ to $O_{3_{\max}}$ (nT)		-38.06 to -37.89		—
	Combined result			
O_3 (nT)			-37.99	
	Combined error bars			
$O_{3_{\min}}$ to $O_{3_{\max}}$ (nT)			-38.06 to -37.89	

Table 4. Example of a zero-level calculation for THEMIS-B. For the filtered case, the cutoff frequency of the high-pass filter is 3.3 mHz. The full set of selection criteria is given in table 1.

	Unfiltered input data		Filtered input data	
	Inversion			
Number of independent points	3302	$>npts = 300$	3425	$>npts = 300$
Number of data windows	215	$>ni = 10$	1915	$>ni = 10$
std(B_3) (nT)	1.835	$>c_2 * mcs = 0.375$	1.259	$>c_2 * mcs = 0.375$
O_3 (nT)		-0.04		-0.09
	Monte Carlo simulation			
abs($O_{3_{\min}} - O_{3_{\max}}$) (nT)	0.233	$<c_3 * mcs = 0.5$	0.257	$<c_3 * mcs = 0.5$
	Result			
O_3 (nT)		-0.04		-0.09
	Error bars			
$O_{3_{\min}}$ to $O_{3_{\max}}$ (nT)		-0.16 to 0.07		-0.22 to 0.04
	Combined result			
O_3 (nT)			-0.07 (average)	
	Combined error bars			
$O_{3_{\min}}$ to $O_{3_{\max}}$ (nT)			-0.22 to 0.07 (worst case of both estimates)	

value for O_3 for the unfiltered case and for the filtered case O_1 and O_3 could not be determined. The criteria that caused the program to dismiss some of the offset calculations are marked in light gray. Since both methods (filtered and unfiltered) did not yield O_3 , our software applied O_1 from the unfiltered case and the averaged O_2 from both cases to the data and reran the algorithm only to solve for O_3 . The outcome of the rerun is displayed in table 3. The algorithm finds O_3 for the unfiltered case. We chose this particular example also to show that the criteria that we choose do not represent strict boundaries between finding accurate and inaccurate calculations. As can be seen in table 3, the estimate of O_3 for the filtered case is being dismissed by the algorithm even though the value of -38.07 nT appears to be very close to the result of the unfiltered case which is -37.99 nT. Our selection criteria are usually on the safe side. After we had applied the calculated offsets to the data, we reran the algorithm for a testing purpose

and all zero levels came out zero ($O_1 = 0.00$ nT, $O_2 = 0.00$ nT, $O_3 = 0.00$ nT). The algorithm is mathematically not iterative; thus, the algorithm will run the second time (with correct offsets) exactly as the first time (same error bars, same offset calculations will be dismissed, etc). Slight differences can arise for the filtered case because the right-hand side and the left-hand side of equation (26) are not exactly equal.

Magnetic field data of THEMIS-B are displayed in figure 6. The data show multiple bow shock crossings. The roughly 7 h long subset of the data that is marked in gray has been selected as input for an offset calculation. The selected data contain several intervals of large upstream waves which do not disturb our algorithm. The result of the offset calculation is displayed in table 4. The length of the error bar of the calculated offset is only 0.29 nT. Because of the use of spin-averaged data, the accuracy of the spin-plane offsets has no influence on the calculation of the spin-axis offset.

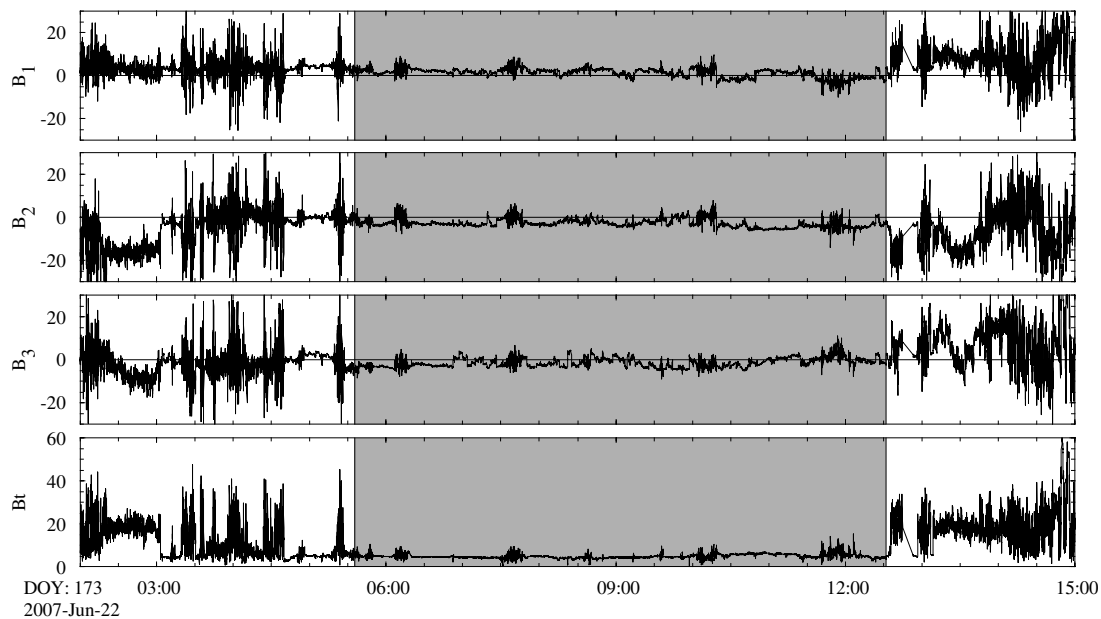


Figure 6. Example of spin-averaged THEMIS-B data. The roughly 7 h long subset that is marked in gray has been used as input for an offset calculation. B_3 represents the spin-plane component. The spin period of the THEMIS spacecraft is roughly 3 s.

The example that we chose for Venus Express uses a slightly different approach. Venus Express had no magnetic cleanliness program. At the positions of the magnetometers, the spacecraft's magnetic field interferes with the natural magnetic field. Initial cleaning of the Venus Express data has been performed (Zhang *et al* 2008) using the gradiometer configuration of the dual triaxial sensors. The initial cleaning of the data provides an ac accuracy of better than 0.1 nT (Zhang *et al* 2008). The inboard sensor is placed directly onto the spacecraft's surface. The outboard sensor is mounted on a short boom of only 1 m in length. The magnetic field strength caused by the spacecraft ranges from 2000 to 6000 nT at the inboard sensor and is roughly 200 nT at the outboard sensor. For Venus Express, we try to detect changes of the zero levels with as rapid a cadence as possible. We apply our whole novel technique using an overlapping 3 h window that is shifted by 1 h. Whenever it is not possible to determine a zero level for a particular component, the window is extended by 1 h toward later times and so on. However, the calculations after the next shift (1 h) again start with a 3 h window (see figures 7(a) and (b)). In order to be able to track offsets, the selection criteria should be such that changes in offset are not mistakenly dismissed as compressions by the algorithm. Table 1 shows the selection criteria that we used for tracking offsets using Venus Express data. The values for mcs , c_2 and c_3 are different from the corresponding values for the other two spacecrafts. A compromise between the accuracy and the tracking ability was made. Large discontinuities of the zero levels occur from one day to the next because the initial data cleaning was done for day-files. An algorithm has been applied (by the data cleaning team) to join the day-files. This algorithm occasionally leaves behind slight jumps in the offsets. We applied our technique using separate day-files so that no windows can cross day-boundaries.

8. Discussion and future work

Because of its mathematical superiority (see section 2.4), the Davis–Smith method represents the method of choice for magnetometer calibrations inside the interplanetary magnetic field. The technique described herein is an improved implementation of the Davis–Smith method. The authors are aware of the fact that there are possibilities of further improving the presented novel technique. We have both documented the mathematical underpinnings of the procedure and explained the relationship to the Belcher technique and the Hedgecock technique and their limitations. These techniques have been used on interplanetary parts of previous missions such as Pioneer Venus (Russell *et al* 1980), Galileo (Kivelson *et al* 1992) and Cassini (Dougherty *et al* 2004) during their interplanetary passages. These zero level calibrations might profit from the application of these techniques herein, but we note that the recalibration must be done on the data in sensor coordinates and not all investigators have chosen to archive data in this coordinate system.

When a spacecraft is in a planetary magnetosheath or even an ICME magnetosheath, the field variations along a component direction may correlate with the magnetic field magnitude for long periods because the shock changes the field only in the direction perpendicular to the shock normal. Inside a planetary magnetosphere a similar situation arises, but with a three-axis stabilized spacecraft rolls or rocking of the spacecraft about its axes can be effective in determining the zero levels. Further studies need to be done for the application of our novel technique to data from rocking or rolling a spacecraft inside a magnetosphere. For example, the change of the Earth's internal field strength at the position of the spacecraft could be filtered out, leaving only the pure rotations of the magnetic field data from rocking or rolling.

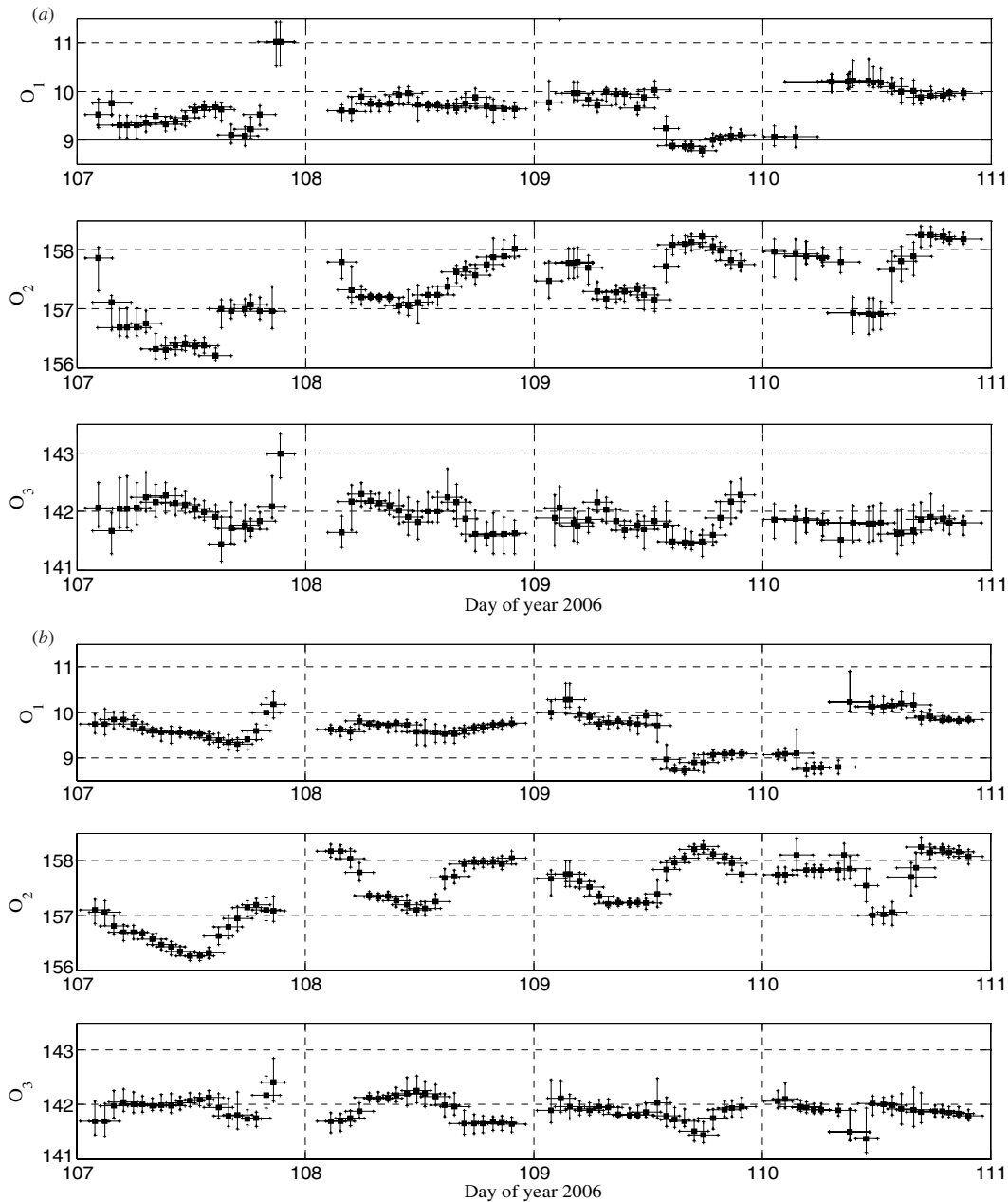


Figure 7. (a) Example of the detection of changing offsets using 4 days of Venus Express data. The input data are unfiltered. The horizontal lines show the timeframe for a particular offset estimate. The vertical black lines represent the error bars for the offset estimates. (b) Example of the detection of changing offsets using 4 days of Venus Express data. The input data are high-pass filtered using a cutoff frequency of 8.9 mHz. The horizontal lines show the timeframe for a particular offset estimate. The vertical lines represent the error bars for the offset estimates.

Additionally, the technique could be applied to purely Alfvénic transverse waves inside a magnetosphere (Cummings *et al* 1969) while filtering out the Earth's internal field. For a spin-stabilized spacecraft this is generally not possible to rock or roll the spacecraft perpendicular to the spin axis, but in multiple spacecraft missions it is sometimes possible to fly with spin axes at a large angle to one another. This was done on ISEE 1 and 2 for brief periods and recently on THEMIS (Angelopoulos). Another technique to obtain the offset of the

third axis is to rotate the sensor along the spin axis into the rotational plane of the spacecraft. This was done on ISEE 1 and 2 (Russell 1978) and Polar (Russell *et al* 1995).

Further work could also be done by validating the presented novel technique using cross-instrument calibrations on a single spacecraft. For example, a vector magnetometer can be calibrated using a reference scalar field strength (Merayo *et al* 2000) such as provided by the gyro-times of an electron drift instrument (e.g. Paschmann *et al* 1997) or

a precise scalar magnetometer. See Olsen *et al* (2003) for information on the scalar calibration of the Ørsted vector magnetometer.

Analysis of the Alfvénic nature of the solar wind (Belcher *et al* 1969) as well as Alfvénic transverse waves inside a magnetosphere (Cummings *et al* 1969) could be done with emphasis on calibration, e.g. for finding ideal frequency bands for zero level determination. These studies could include data from particle instruments as well. For further information, see e.g. Tsurutani and Ho (1999) and Russell (2000).

Acknowledgments

H K Leinweber wishes to thank S Joy, R Walker, K Khurana and M Kivelson for discussions at an early stage of the development of this technique. Work on the STEREO mission was supported by the National Aeronautics and Space Administration under grant NAS5-00133. Work on the Venus Express mission was supported by the National Aeronautics and Space Administration under grant NNG06GC62G. Work on the THEMIS mission was supported under NASA contract NAS5-02099. We acknowledge K H Glassmeier, U Auster and W Baumjohann for the use of FGM data. The FGM data were provided under the lead of the Technical University of Braunschweig and with financial support through the German Ministry for Economy and Technology and the German Center for Aviation and Space (DLR) under contract 50 OC 0302.

References

- Acuña M H 2002 Space-based magnetometers *Rev. Sci. Instrum.* **73** 3717
- Altschuler M D, Levine R H, Stix M and Harvey J 1977 High resolution mapping of the magnetic field of the solar corona *Solar Phys.* **51** 345
- Angelopoulos V 2007 private communication
- Belcher J W 1973 A variation of the Davis–Smith method for in-flight determination of spacecraft magnetic fields *J. Geophys. Res.* **78** 6480
- Belcher J W, Davis L Jr and Smith E J 1969 Large amplitude Alfvén waves in the interplanetary medium: Mariner 5 *J. Geophys. Res.* **77** 2302
- Coleman P J Jr 1966 Variations in the interplanetary magnetic field: Mariner 2. 1. Observed properties *J. Geophys. Res.* **71** 5509
- Cummings W D, O’Sullivan R J and Coleman P J 1969 Standing Alfvén waves in the magnetosphere *J. Geophys. Res.* **74** 778–93
- Davis L Jr and Smith E J 1968 The in-flight determination of spacecraft magnetic field zeros *EOS Trans. AGU* **49** 257
- Dougherty M *et al* 2004 The Cassini magnetic field investigation *Space Sci. Rev.* **114** 331–83
- Efron B 1982 *The Jackknife, the Bootstrap, and other Resampling Plans* (Philadelphia: SIAM)
- Farrell W M, Thompson R F, Lepping R P and Byrnes J B 1995 A method of calibrating magnetometers on a spinning spacecraft *IEEE Trans. Magn.* **31** 996
- Hedgecock P C 1975 A correlation technique for magnetometer zero level determination *Space Sci. Instrum.* **1** 83–90
- Kepko E L, Khurana K K and Kivelson M G 1996 Accurate determination of magnetic field gradients from four point vector measurements: I. Use of natural constraints on vector data obtained from a single spinning spacecraft *IEEE Trans. Magn.* **32** 377
- Kivelson M G, Khurana K K, Means J D, Russell C T and Snare R C 1992 The Galileo magnetic field investigation *Space Sci. Rev.* **60** 357–83
- Merayo J M G, Brauer P, Primdahl F, Petersen J R and Nielsen O V 2000 Scalar calibration of vector magnetometers *Meas. Sci. Technol.* **11** 120–32
- Ness N F and Burlaga L F 2001 Spacecraft studies of the interplanetary magnetic field *J. Geophys. Res.* **106** 15803
- Ness N F, Scarce C S and Seek J B 1964 Initial results of the IMP-1 magnetic field experiment *J. Geophys. Res.* **69** 3531
- Olsen N, Toffner-Clausen L, Sabaka T J, Brauer P, Merayo J M G, Jorgensen J L, Leger J M, Nielsen O V, Primdahl F and Risbo T 2003 Calibration of the Ørsted vector magnetometer *Earth Planets Space* **55** 11–8
- Paschmann G *et al* 1997 The electron drift instrument for cluster *Space Sci. Rev.* **79** 233–69
- Rosenberg R L 1971 *Automatic Calculation of Zero Levels for Interplanetary Spacecraft Magnetometers by the Davis Method* Publ. No. 903, Institute of Geophysics and Planetary Physics, UCLA
- Russell C T 1978 The ISEE1 and ISEE2 fluxgate magnetometer *IEEE Trans. Geosci. Electron.* **GE-16** 239–42
- Russell C T 2000 The solar wind interaction with the earth’s magnetosphere: a tutorial *IEEE Trans. Plasma Sci.* **28** 1818–30
- Russell C T, Snare R C, Means J D and Elphic R C 1980 Pioneer Venus Orbiter fluxgate magnetometer *IEEE Trans. Geosci. Remote Sens.* **GE-18** 32–6
- Russell C T, Snare R C, Means J D, Pierce D, Dearborn D, Larson M, Barr G and Le G 1995 The GGS/polar magnetic fields investigation *Space Sci. Rev.* **71** 563–82
- Snare R C 1998 A history of Vector magnetometry in space *AGU, Geophys. Monogr.* **103** 101
- Sonnerup B U Ö and Cahill L J 1967 Magnetopause structure and attitude from Explorer 12 observations *J. Geophys. Res.* **72** 171
- Tsurutani B T and Ho C M 1999 A review of discontinuities and Alfvén waves in interplanetary space: Ulysses results *Rev. Geophys.* **37** 517–41
- Zhang T L *et al* 2008 Initial Venus Express magnetic field observations of the Venus bow shock location at solar minimum *Planet. Space Sci.* at press doi: [10.1016/j.pss.2007.09.012](https://doi.org/10.1016/j.pss.2007.09.012)